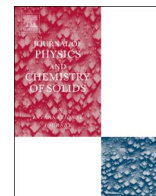




ELSEVIER

Contents lists available at ScienceDirect

## Journal of Physics and Chemistry of Solids

journal homepage: [www.elsevier.com/locate/jpcs](http://www.elsevier.com/locate/jpcs)The high-pressure compressibility of  $B_{12}P_2$ 

HPSTAR  
485-2017

 Yang Gao<sup>a</sup>, Mi Zhou<sup>a,b</sup>, Haiyan Wang<sup>a,c</sup>, Cheng Ji<sup>d</sup>, C.E. Whiteley<sup>e</sup>, J.H. Edgar<sup>e</sup>, Haozhe Liu<sup>f</sup>,  
 Yanzhang Ma<sup>a,\*</sup>
<sup>a</sup> Texas Tech University, Department of Mechanical Engineering, Lubbock, TX 79409, USA<sup>b</sup> Jilin University, Department of Physics, Changchun 130012, PR China<sup>c</sup> Zhengzhou University of Light Industry, School of Physics and Electronic Engineering, Zhengzhou 450002, PR China<sup>d</sup> High Pressure Synergetic Consortium, Advanced Photon Source, Argonne National Laboratory, 9700 S. Cass Ave., Bldg. 401, Lemont, IL 60439, USA<sup>e</sup> Kansas State University, Department of Chemical Engineering, Manhattan, KS 66506, USA<sup>f</sup> Center for High Pressure Science & Technology Advanced Research, Changchun 130015, PR China

## A B S T R A C T

*In situ* high pressure synchrotron X-ray diffraction measurements were performed on icosahedral boron phosphide ( $B_{12}P_2$ ) to 43.2 GPa. No structural phase transition occurs over this pressure range. The bulk modulus of  $B_{12}P_2$  is  $K_{OT} = 207 \pm 7$  GPa with pressure derivative of  $K'_{OT} = 6.6 \pm 0.8$ . The structure is most compressible along the chain formed by phosphorus and boron atoms in the crystal structure. It is believed that the compressibility of boron-rich compounds at close to ambient pressure is determined by the boron icosahedral structure, while the inclusive atoms (both boron and non-boron) between the icosahedra determine the high-pressure compressibility and structure stability.

## 1. Introduction

Boron and boron-rich compounds are of interest for their extreme properties such as their high hardness, chemical inertness, good thermal stability, and resistance to radiation damage. [1–26] These properties are a consequence of their unusual chemical bonding: it contains unusual “electron deficient” bonds, the 2-electron-3-center bond, where one pair of electrons are shared among three atoms. [1,5] As a result, the boron atoms tends to form various types of chains and clusters, for example a twelve boron atom icosahedra, in elemental boron and boron-rich compounds. The boron icosahedra are piled together in a close packed arrangement, and when other elements are present, they fit in the gaps between icosahedra. The structure of  $B_{12}P_2$  (shown in Fig. 1(a)) is similar to other rhombohedral elemental boron and other boron-rich compounds such as boron carbide and boron suboxide. [23,25] Eight boron icosahedra occupy each vertexes of the rhombohedron and a chain of two phosphorus atoms occupy the body diagonal of the rhombohedron. The two phosphorus atoms are bonded together and to three boron icosahedra assembled along the *a*- and *b*-axis. Previous Raman studies have reported that  $B_{12}P_2$  experience no structural phase transition until 80 GPa before a reversible transition

to a distorted structure is caused by the deformation of the icosahedral structures. [7].

Due to the close-pack structure of these icosahedra based boron-rich compounds, high hardness is usually expected. Boron carbide, for example, is the third hardest material in nature next to diamond and cubic boron nitride, yet brittleness has significantly limited its application. [26–28] Recently, An and Goddard predicted that boron suboxide ( $B_6O$ ) and icosahedral boron phosphide ( $B_{12}P_2$ ) should be much less brittle than boron carbide due to their ability to reform bonds between planes as they slip past each other. [10] In contrast, boron carbide does not have this ability. Thus  $B_6O$  and  $B_{12}P_2$  may be superior to boron carbide in applications in which the material is subjected to high strain rates such as in armor.

To better assess whether  $B_{12}P_2$  might be useful in such applications, it is necessary to better establish its physical and mechanical properties. Previously, using an *ab initio* method with density functional theory (DFT), Gao et al. [29] predicted the bulk moduli of  $B_{12}P_2$  and  $B_{12}As_2$  as 208.3 GPa and 204.6 GPa, respectively. Using the *in-situ* high-pressure x-ray diffraction which we reported here, Wu et al. [24] measured the bulk modulus of  $B_{12}As_2$  (a compound similar in structure to  $B_{12}P_2$ ) as 204 GPa. The present study was undertaken to experi-

\* Corresponding author.

E-mail address: [y.ma@ttu.edu](mailto:y.ma@ttu.edu) (Y. Ma).

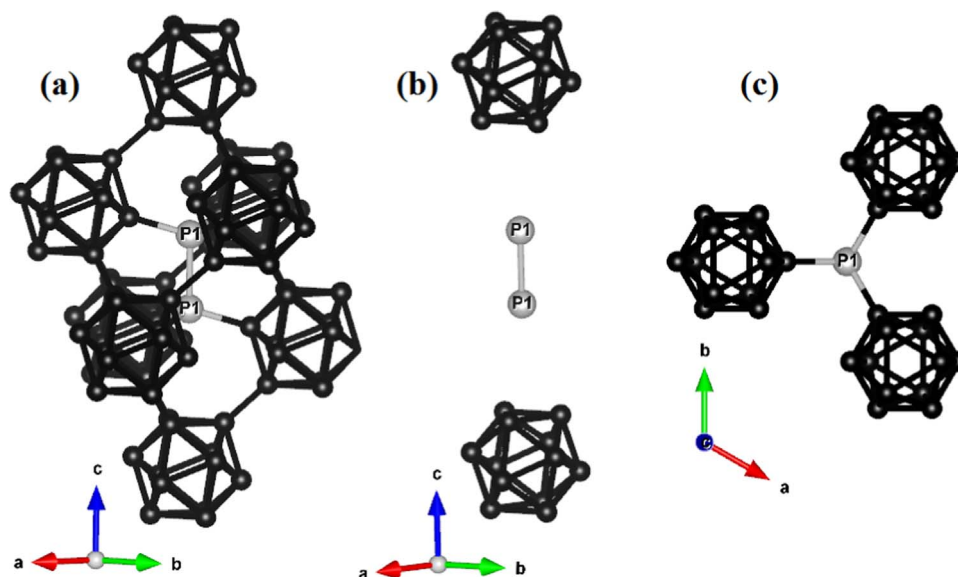


**Fig. 1.** The crystal structure of  $B_{12}P_2$ . The black and grey spheres represent the boron and phosphorus atoms, respectively. (a) the unit-cell of  $B_{12}P_2$ ; (b) the chained structure of  $B_{12}P_2$  along  $c$ -axis; (c) the tetrahedral structure of  $B_{12}P_2$  assembled along  $a$ -axis (looking from  $c$ -axis).

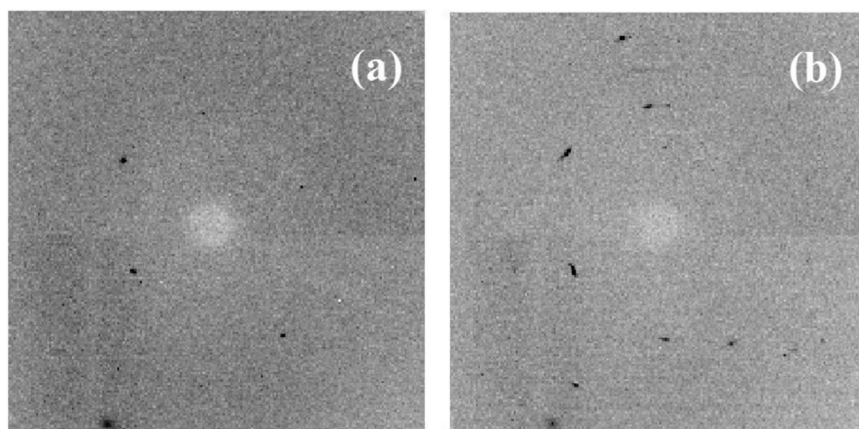


**Fig. 2.** X-ray diffraction images of  $B_{12}P_2$  at pressures. (a) at 0.4 GPa, (b) at 43.2 GPa.

mentally measure the bulk modulus of icosahedral boron phosphide, and to compare with relevant compounds to reveal their common behavior under pressure influence.

## 2. Experiment details

The icosahedral boron phosphide ( $B_{12}P_2$ ) crystals were produced by dissolving cubic boron phosphide (BP) powder in molten nickel at 1350 °C under a flow of phosphine, then slowly cooling to 1000 °C. During the cooling process, the  $B_{12}P_2$  crystals precipitated instead of BP, due to the loss of phosphorus. The solidified nickel flux was removed by etching in acid.

A symmetric diamond anvil cell was employed for pressure generation. A pair of 400- $\mu\text{m}$  flat culet diamond anvils was selected.

A sheet of rhenium was pre-indented to 43  $\mu\text{m}$  with a hole of 150  $\mu\text{m}$  in diameter being drilled in the center of the indentation by a laser drilling device. A chip of  $B_{12}P_2$  sample was loaded into the sample chamber with two ruby spheres aside for pressure calibration. Neon gas was also loaded in the sample chamber as pressure transmitting medium. The x-ray diffraction experiment was performed at 13-BMD station of Advanced Photon Source (APS), Argonne National Laboratory (ANL). The x-ray wavelength was 0.3344 Å. A Mar165 CCD detector recorded the diffraction images, which were processed and analyzed using Dioptas. [30] The integrated diffraction patterns were used to determine the diffraction peaks with peakfit and the refinement was done by UNITCELL. [31] Due to the nature of the sample (multiple crystals) and the resultant limited number of diffraction peaks, positional refinement was not performed during analysis.

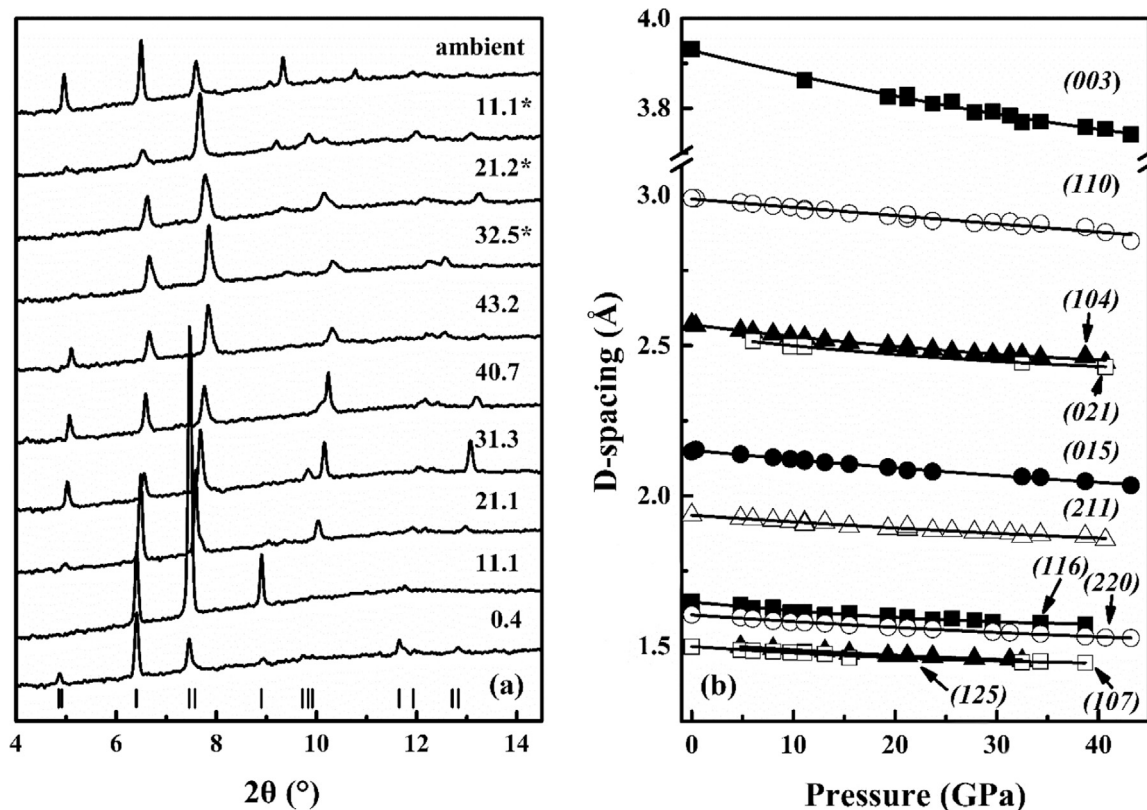


**Fig. 3.** (a) Integrated x-ray diffraction patterns of  $B_{12}P_2$  under pressures. Star, pattern acquired during decompression, vertical bar, the reference diffraction peak position, and numbers on the curve, pressure in GPa. (b) Pressure dependence of d-spacings of  $B_{12}P_2$ . The numbers marked aside the lines are the corresponding Miller indices..

### 3. Result and discussion

From the diffraction images (shown in Fig. 2), diffraction spots can be clearly observed, indicating that the sample was initially a single crystal and broke into a number of smaller single crystal pieces as pressure was elevated. At different pressure the position of the diffraction spots varies, which may be caused by the reorientation of the crystals in the sample chamber. Fig. 3(a) shows the integrated x-ray diffraction patterns of  $B_{12}P_2$  at selected pressures. No anomaly related to structure change is observed during compression and decompression processes, thus there is no structural phase transition over the tested pressure range. Fig. 3(b) displays the variation of d-spacings of the sample with pressures. The d-spacings of  $B_{12}P_2$  consistently decrease with increasing pressures. The relative intensity variations, as well as the appearance and disappearance of peaks may be caused by the crystal reorientation in the sample chamber under pressure.

The pressure dependence of the cell parameters is presented in Fig. 4 and the specific cell parameters and unit-cell volumes under pressure are listed in Table 1. Since at each pressure that all peaks observed are used in the cell parameter refinements and that the variation of the number of peaks and their intensities are observed, the refined cell parameters show scattering at pressures. It is observed, that the  $B_{12}P_2$  is slightly more compressible along  $c$ -axis than  $a$ -axis at lower pressures, and this anisotropy continuously increases with pressure elevation. At 43.2 GPa, the axial compression rate differs by

33.7%. Thus,  $B_{12}$ -P-P- $B_{12}$  chain (shown in Fig. 1(b)) along the  $c$ -direction, is more compressible than other spacial configurations of atoms (shown in Fig. 1(c)). Such compressible anisotropy was also seen with  $B_{12}As_2$  [24] and  $\beta$ -boron, where the  $B_{12}$ -As-As- $B_{12}$  and the  $B_{12}$ - $B_{10}$ -B- $B_{10}$ - $B_{12}$  chain structures are much more compressible.

It is also observed that, lattice parameters in the decompression process diverge from those in compression (shown in Fig. 5). When decompressed from 43.2 GPa, the compressibility curve of  $a$ -axis is slightly below its compression curve. The  $c$ -axis has opposite behavior above 11.1 GPa. This sluggish recovery from compression along the  $c$ -axis also indicates the weakness of bonding along the P-P chain. Hence the application of high pressure exerts a larger impact on the chained structure than the boron icosahedra. Inclusion of the compressibility anisotropy above, the  $B_{12}$  icosahedral structure is more rigid in  $B_{12}P_2$ , which is consistent with observation in  $\beta$ -boron and  $B_{12}As_2$  [24]. This may indicate that the boron icosahedral structure has low (possibly the lowest) energy structural configuration.

The pressure dependence of unit-cell volumes of  $B_{12}P_2$  are shown in Fig. 6. The volume is reduced by 12.4% as the pressure increases from 0.1 to 43.2 GPa. Fitting the data to 2nd order Birch-Murnaghan [32,33] equation of state yield a bulk modulus of  $K_{OT} = 234 \pm 3$  GPa, while the 3rd order equations of state yield a bulk modulus of  $K_{OT} = 207 \pm 7$  GPa and its pressure derivative  $K'_{OT} = 6.6 \pm 0.8$ . As shown in Fig. 6, regarding the distribution of data points and the fitted curves, the 3rd order model has demonstrated a better fit than the 2nd

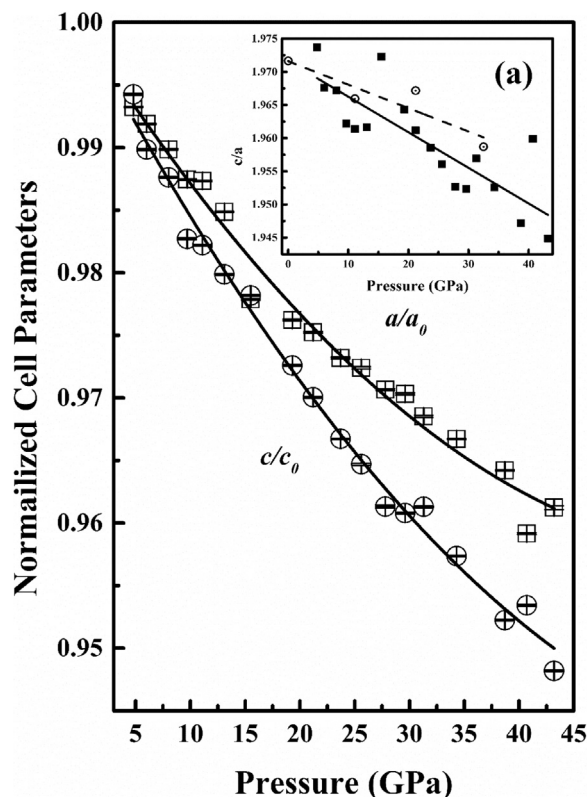


**Fig. 4.** The pressure dependence of cell parameters of  $B_{12}P_2$ . The lines are the fitting results. The error bars represent the error resulted during the refinement. Inset (a): the pressure dependence of  $c/a$  ratio. Open circle, decompression data; solid square, compression data; dashed lines, decompression curve; black lines, compression curve. (the large error is resulted from the refinement yet it is realized that the different number of  $d$ -spacings adopted in the refinement can cause the data scattering).

order model. Thus the ambient pressure bulk modulus of  $B_{12}P_2$  is determined to be 207 GPa, which is in good agreement to the value predicted by Gao *et al.* [29].

The unit-cell volumes of  $B_{12}P_2$  as a function of pressure are shown in Fig. 7 along with those of  $\alpha$ - and  $\beta$ -rhombohedral boron and  $B_{12}As_2$  for comparison (Birch-Murnaghan equation of state for  $B_{12}P_2$ ,  $\beta$ -boron, and  $B_{12}As_2$ , Vinet [34] equation of state for  $\alpha$ -boron). As shown in Table 2, the ambient pressure bulk moduli for each material are 207.1 GPa for  $\alpha$ -boron [6], 205 GPa for  $\beta$ -rhombohedral boron [9], 204 GPa for  $B_{12}As_2$  [24], and 207 GPa for  $B_{12}P_2$ . Considering the uncertainty, the bulk moduli of these materials are considered identical. Yet the volume reduction value of  $B_{12}P_2$  is clearly lower than these materials, indicating the lower compressibility of  $B_{12}P_2$  at high pressures. Fig. 7 inset (a) are the high-pressure bulk moduli of  $B_{12}P_2$ ,  $\alpha$ - and  $\beta$ -boron and  $B_{12}As_2$  based on their pressure derivatives (shown in Table 2). It is discovered that  $B_{12}P_2$  and  $B_{12}As_2$  are respectively the most and least rigid at high pressures, while  $\alpha$ - and  $\beta$ -boron have almost identical bulk moduli through the pressure range.

It was previously determined by Wu *et al.* [24] that the boron icosahedral structures play a dominant role in compressibility for boron-rich compounds based on the comparison of the bulk modulus of  $B_{12}As_2$  to that of  $\beta$ -boron. An and Goddard's<sup>10</sup> theoretical study also predicted that the specific configuration of the doping structures incorporated inside the rhombohedral cage of boron icosahedra is also a major factor influencing the shear strength of such boron-rich

**Table 1**

The cell parameters and unit-cell volumes of  $B_{12}P_2$  at pressures.

$P$ (GPa)	$a$ (Å)	$c$ (Å)	$V$ (Å <sup>3</sup> )
0.0 <sup>a</sup>	5.9930(3)	11.8161(7)	367.53(4)
4.8	5.9525(3)	11.7482(7)	360.49(4)
6.0	5.9444(3)	11.6962(8)	357.92(4)
8.0	5.9322(3)	11.6699(7)	355.65(4)
9.7	5.9178(3)	11.6118(7)	352.17(4)
11.1	5.9171(3)	11.6058(7)	351.90(4)
11.1 <sup>a</sup>	5.9055(3)	11.610(1)	350.64(5)
13.1	5.9023(3)	11.5783(7)	349.32(4)
15.5	5.8604(3)	11.5583(7)	343.78(4)
19.3	5.8505(4)	11.4923(7)	340.67(5)
21.2	5.8446(4)	11.4623(7)	339.09(4)
21.2 <sup>a</sup>	5.8417(4)	11.4916(7)	339.62(5)
23.7	5.8323(4)	11.4230(5)	336.50(5)
25.6	5.8276(6)	11.340(3)	335.28(6)
27.8	5.8172(4)	11.359(1)	332.89(5)
29.6	5.8151(5)	11.3529(7)	332.46(5)
31.3	5.8044(5)	11.3588(8)	331.42(5)
32.5 <sup>a</sup>	5.7840(3)	11.3291(7)	328.23(3)
34.3	5.7935(3)	11.3123(6)	328.82(4)
38.7	5.7785(3)	11.2518(6)	325.38(4)
40.7	5.7482(4)	11.2657(7)	322.36(4)
43.2	5.7607(9)	11.2038(8)	322.00(9)

<sup>a</sup> Data points acquired during decompression process.

compounds. The present results further indicate that the compressibility is mainly determined by the  $B_{12}$  icosahedra at ambient pressure and by the structure and component of elements (other than boron in the form of  $B_{12}$  icosahedra) in the body diagonal of the rhombohedral structure at high pressures. It is interesting that these chained atoms in the rhombohedral boron-rich compounds affect and only affect the high-pressure compressibility. It may be a clue for design and synthesis of boron-rich materials with superior high-pressure performance.

#### 4. Conclusion

X-ray diffraction experiments on  $B_{12}P_2$  were performed to 43.2 GPa in a diamond anvil cell. There is no phase transition in the pressure range. As pressure elevation,  $c$ -axis is more compressible than  $a$ -axis. The bulk modulus of  $B_{12}P_2$  is 207 GPa. By comparison of  $B_{12}P_2$ ,  $B_{12}As_2$ ,  $\alpha$ -, and  $\beta$ -boron, it is believed that the compressibility of boron-rich compounds is determined by the boron icosahedral structure at close to ambient pressure while the inclusive atoms (both boron and non-boron) in non-icosahedral structure determine the high pressure compressibility and structural stability.

#### Acknowledgement

The authors thank the gas loading assistant and technical support by Dr. Sergey Tkachev at GESE CARS in APS, ANL. This research is supported by National Science Foundation (DMR1431570, program manager, John Schlueter), Defense Advanced Research Project Agency (W31P4Q-13-1-0010, program manager, Judah Goldwasser), and Army Research Office (W911NF-09-1-0001, program manager, David Stepp and Suveen Mathaudhu). This research is also supported by Department of Energy Grant No. GEGF001846.

The authors would also like to thank the anonymous reviewer for the professional insight reviewing this paper.

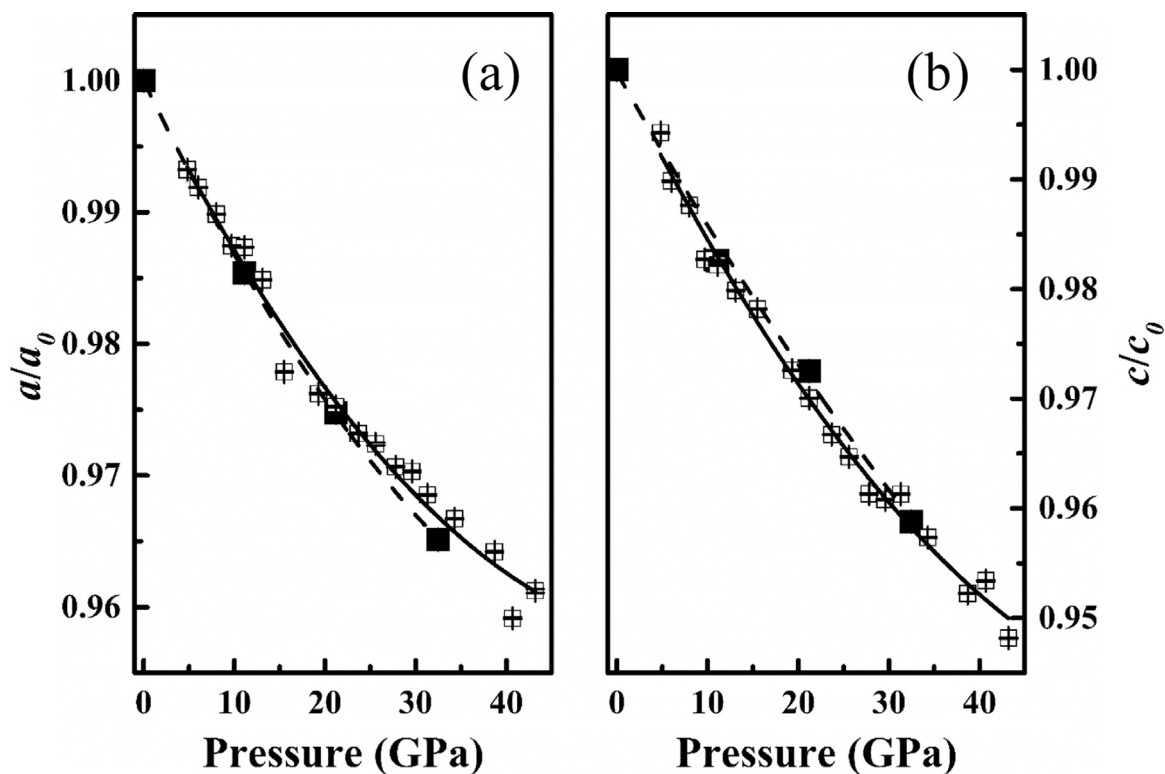


Fig. 5. The pressure dependence of cell parameters of  $B_{12}P_2$  from compression and decompression, (a)  $a/a_0$ , (b)  $c/c_0$ . Open square, compression data; solid square, decompression data; solid lines, compression curve; dashed lines, decompression curve. The error bars represent the error resolved during the refinement (the large error is resulted from the refinement yet it is realized that the different number of d-spacings adopted in the refinement can cause the data scattering).

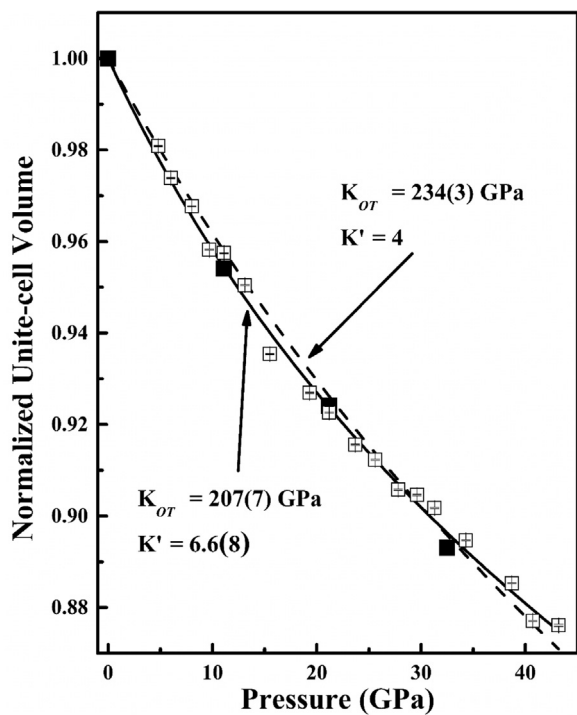


Fig. 6. The pressure dependence of unit-cell volume of  $B_{12}P_2$ . The solid squares represent the data from decompression. The error bars represent the error resulted during the refinement (the large error is resulted from the refinement yet it is realized that the different number of d-spacings adopted in the refinement can cause the data scattering).

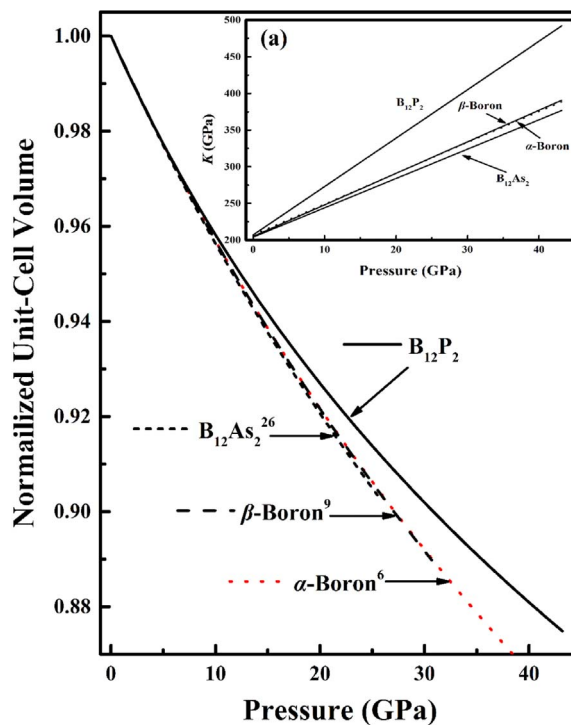


Fig. 7. Comparison of the pressure dependent unit-cell volume of  $B_{12}P_2$ ,  $B_{12}As_2$ ,  $\alpha$ - and  $\beta$ -boron. The pressure dependence of bulk moduli for  $B_{12}P_2$ ,  $B_{12}As_2$ ,  $\beta$ -boron and  $\alpha$ -boron is shown in inset (a).

**Table 2**

The bulk moduli and their pressure derivatives for some solid boron and boron-rich compounds.

Material	Bulk modulus (GPa)	Pressure derivative
$\alpha$ -rhombohedral boron (Ref [6])	207.1 (12.8)	4.2 (0.3)
$\beta$ -rhombohedral boron (Ref [9])	205 (16)	4.3 (1.6)
B <sub>12</sub> As <sub>2</sub> (Ref [24])	204 (1)	4
B <sub>12</sub> P <sub>2</sub>	207 (7)	6.6 (0.8)

## References

- [1] D. Emin, *Phys. Today* 40 (1987).
- [2] R. Nelmes, J. Loveday, D. Allan, J. Besson, G. Hamel, P. Grima, S. Hull, *Phys. Rev. B* 47 (1993) 7668.
- [3] A. Masago, K. Shirai, H. Katayama-Yoshida, *Phys. Rev. B* 73 (2006) 104102.
- [4] D. Li, W. Ching, *Phys. Rev. B* 52 (1995) 17073.
- [5] D. Emin, *J. Solid State Chem.* 179 (2006) 2791.
- [6] A. Polian, J. Chervin, P. Munsch, M. Gauthier, In  $\alpha$ -boron at Very High Pressure: Structural and Vibrational Properties, *Journal of Physics: Conference Series*, IOP Publishing, Bristol, UK, Vol. 121, Part 4; (2008) 042017
- [7] S.V. Ovsyannikov, A. Polian, P. Munsch, J.-C. Chervin, G. Le Marchand, T.L. Aselage, *Phys. Rev. B* 81 (2010) 140103.
- [8] A.R. Oganov, J. Chen, C. Gatti, Y. Ma, Y. Ma, C.W. Glass, Z. Liu, T. Yu, O.O. Kurakevych, V.L. Solozhenko, *Nature* 457 (2009) 863.
- [9] Y. Ma, C.T. Prewitt, G. Zou, H.-k. Mao, R.J. Hemley, *Phys. Rev. B* 67 (2003) 174116.
- [10] Q. An, W.A. Goddard III, *Chem. Mater.* 27 (2015) 2855.
- [11] J. Hoard, D. Sullenger, C. Kennard, R. Hughes, *J. Solid State Chem.* 1 (1970) 268.
- [12] G.A. Slack, T. McNelly, E. Taft, *J. Phys. Chem. Solids* 44 (1983) 1009.
- [13] I. Morrison, D. Bylander, L. Kleinman, *Phys. Rev. B* 45 (1992) 1533.
- [14] M. Carrard, D. Emin, L. Zuppiroli, *Phys. Rev. B* 51 (1995) 11270.
- [15] N. Vast, S. Baroni, G. Zerah, J. Besson, A. Polian, M. Grimsditch, J. Chervin, *Phys. Rev. Lett.* 78 (1997) 693.
- [16] I. HIGASHI, T. ISHII, *Forma* 16 (2001) 187.
- [17] K. Shirai, A. Masago, H. Katayama-Yoshida, *Phys. Status Solidi (b)* 241 (2004) 3161.
- [18] E.Y. Zarechnaya, L. Dubrovinsky, N. Dubrovinskaia, N. Miyajima, Y. Filinchuk, D. Chernyshov, V. Dmitriev, *Sci. Technol. Adv. Mater.* (2008).
- [19] E.Y. Zarechnaya, L. Dubrovinsky, N. Dubrovinskaia, Y. Filinchuk, D. Chernyshov, V. Dmitriev, N. Miyajima, A. El Goresy, H. Braun, S. Van Smaalen, *Phys. Rev. Lett.* 102 (2009) 185501.
- [20] A.R. Oganov, V.L. Solozhenko, C. Gatti, O.O. Kurakevych, Y. Le Godec, *J. Superhard Mater.* 33 (2011) 363.
- [21] Y. Le Godec, M. Mezouar, O.O. Kurakevych, P. Munsch, U. Nwagwu, J.H. Edgar, V.L. Solozhenko, *J. Superhard Mater.* 36 (2014) 61.
- [22] V.L. Solozhenko, V.A. Mukhanov, P.S. Sokolov, Y.L. Godec, K.A. Cherednichenko, Z. Konôpková, arXiv preprint arXiv:1601.02930, 2016.
- [23] B. Morosin, A. Mullendore, D. Emin, G. Slack, *Rhombohedral Crystal Structure of Compounds Containing Boron-rich Icosahedra*, AIP Publishing, Albuquerque, NM, USA, 1986, p. 70.
- [24] J. Wu, H. Zhu, D. Hou, C. Ji, C. Whiteley, J. Edgar, Y. Ma, *J. Phys. Chem. Solids* 72 (2011) 144.
- [25] Z. Liu, J. Kawamura, M. Nagasono, K. Maeda, J. Kawai, *J. Electron Spectrosc. Relat. Phenom.* 135 (2004) 73.
- [26] Q. An, W.A. Goddard III, T. Cheng, *Phys. Rev. Lett.* 113 (2014) 095501.
- [27] X. Yan, Z. Tang, L. Zhang, J. Guo, C. Jin, Y. Zhang, T. Goto, J. McCauley, M. Chen, *Phys. Rev. Lett.* 102 (2009) 075505.
- [28] M. Chen, J.W. McCauley, K.J. Hemker, *Science* 299 (2003) 1563.
- [29] F. Gao, L. Hou, Y. He, *J. Phys. Chem. B* 108 (2004) 13069.
- [30] C. Prescher, V.B. Prakapenka, *High. Press. Res.* 35 (2015) 223.
- [31] T. Holland, S. Redfern, *J. Appl. Crystallogr.* 30 (1997) 84.
- [32] F.D. Murnaghan, *Am. J. Math.* 59 (1937) 235.
- [33] F. Birch, *Phys. Rev.* 71 (1947) 809.
- [34] P. Vinet, J.H. Rose, J. Ferrante, J.R. Smith, *J. Phys.: Condens. Matter* 1 (1989) 1941.